



# A highly fluorescent lanthanide metal-organic framework as dual-mode visual sensor for berberine hydrochloride and tetracycline

Jie Xiong<sup>1</sup> · Lu Yang<sup>1</sup> · Li Xia Gao<sup>1</sup> · Pan Pan Zhu<sup>1</sup> · Qian Chen<sup>1</sup> · Ke Jun Tan<sup>1</sup>

Received: 23 May 2019 / Revised: 14 June 2019 / Accepted: 27 June 2019 / Published online: 13 July 2019  
© Springer-Verlag GmbH Germany, part of Springer Nature 2019

## Abstract

A microscale highly fluorescent Eu metal-organic framework (Eu-MOF) was synthesized with terephthalic acid and 1H-1,2,4-triazole-3,5-diamine by one-pot hydrothermal method. And it was characterized by scanning electron microscope, Fourier transform infrared spectroscopy, powder X-ray diffraction, fluorescence spectroscopy, thermogravimetric analysis, and energy dispersive X-ray mapping. The prepared Eu-MOF has high quantum yield of 30.99%, excellent water dispersibility, good fluorescence stability, and favorable thermal stability. Based on the distinctly different fluorescence responses of different emission, the prepared Eu-MOF was used as dual-mode visual sensor for the sensitive detection of berberine hydrochloride and tetracycline. The limits of detection are 78 nM and 17 nM, respectively. The sensing mechanism was also discussed. Moreover, a filter paper sensor has been designed for sensing tetracycline with a notable fluorescence color change from blue to red. The prepared Eu-MOF is promising to be developed as a multi-mode luminescent sensor for visual detection in biochemical analysis.

**Keywords** Metal-organic framework · Dual-mode sensor · Visual detection · Berberine hydrochloride · Tetracycline

## Introduction

Berberine hydrochloride (BRH) and tetracycline (TC) are both anti-bacterial drugs and widely used in clinical treatment. BRH is a major effective content of phellodendron bark and coptis rhizome. It has been proved to have a wide pharmacokinetic activity, such as anti-inflammatory [1], anti-diabetic [2], anti-tumor [3], anti-bacterial [4], and anti-depressant [5]. Hence, the quantification of berberine hydrochloride is particularly vital. At present, some analytical methods have been established for the determination of BRH, including high-performance liquid

chromatography (HPLC) [6], chemifluorescence [7], colorimetric [8], capillary electrophoresis [9], and light scattering spectrometry [10]. TC is a broad-spectrum antibiotic, which can disturb protein synthesis of bacteria to inhibit bacterial activity. TC is used as food additives for the treatment of animal growth in stockbreeding [11], and it can also treat the bacterial infections in humans and animals. However, the overuse of TC has resulted in a series of problems such as antibiotic accumulation and the increasing emergence of antibiotic resistance [12]. Thereby, it is necessary to develop efficient methods for the detection of TC. Up to now, TC has various analytical methods, such as high-performance liquid chromatography (HPLC) [13], capillary electrophoresis (CE) [14], liquid chromatograph with tandem mass spectrometry (LC-MS) [15], electrochemical analysis [16], immune assay (IA) [17], and colorimetric [18]. Most of these technologies for BRH and TC sensing suffered time-consuming, expensive instrument and sophisticated sample pretreatment. To overcome these difficulties, fluorescence method [19, 20] is a desirable method due to the easy fabrication, facile manipulation, low cost, and obvious fluorescence color change.

**Electronic supplementary material** The online version of this article (<https://doi.org/10.1007/s00216-019-02004-9>) contains supplementary material, which is available to authorized users.

✉ Ke Jun Tan  
tankj@swu.edu.cn

<sup>1</sup> Key Laboratory of Luminescent and Real-Time Analytical Chemistry (Southwest University), Ministry of Education, College of Chemistry and Chemical Engineering, Southwest University, No. 1 Tiansheng Road, Beibei District, Chongqing 400715, China

Metal-organic frameworks (MOFs) as a class of multi-functional hybrid materials have achieved a broader development in gas separation [21], storage [22], catalysis [23], and chemical sensing [24, 25]. Lanthanide metal-organic frameworks (Ln-MOFs), an important fluorescence material, have attracted considerable attentions owing to unique luminescent properties like large Stokes shift, long decay lifetime, and characteristically narrow emission spectra [26]. Ln-MOFs are mainly composed of lanthanide ions and organic ligands. Therefore, Ln-MOFs can be implemented as multi-functional fluorescence sensors based on the fluorescence change of lanthanide ions or appropriate ligands [27]. However, the fluorescence intensity of Ln-MOFs is usually weak because of the existence of forbidden f-f transition, unless an appropriate ligand function as “antenna” to effectively transfer the energy or some pre-designs, one-pot synthesis and post-modifications are taken to strength the “antenna effect” [28]. In most cases, the fluorescence sensing of Ln-MOFs is mainly based on the monotonous quenching or enhancement of fluorescence intensity [29], which is easily affected by some inevitable factors, such as system noise and source instability. Besides, the fluorescence color change is hardly distinguished by the naked eyes. From this viewpoint, visual detection based on ratiometric fluorescent sensing is a wise consideration for the good accuracy and sensitive color change [30]. Analytical tests using color changes as readout provide great convenience because they can be read without instruments [31]. In recent years, due to their tunable pores and prominent luminescent properties, Ln-MOFs were developed as fluorescent sensing platform for the sensing of ions [32], biomarkers [33], small molecules [34], temperature [35], pH [36], and so on. However, few reports can be found about the visual sensing of TC and BRH based on Ln-MOFs.

In this work, a dual-mode europium metal-organic framework (Eu-MOF 1) probe was synthesized with Eu (III) ions as metal node and terephthalic acid as main functional ligand. In addition, 1H-1,2,4-triazole-3,5-diamine (Hdatrz) was employed to improve the fluorescence behavior of Eu-MOF 1 via one-pot hydrothermal method. The prepared Eu-MOF 1 has excellent luminescent properties, thermal stability, and fluorescence stability in water. The results indicate that Eu-MOF 1 can be developed as a fluorescence sensor based on obvious fluorescence change in aqueous solution. It is found that Eu-MOF 1 exhibits strong emission of  $\text{Eu}^{3+}$  when excited at 280 nm, which can be quenched by BRH. More interestingly, Eu-MOF 1 shows ligand-center emission and weak  $\text{Eu}^{3+}$  emission when excited at 365 nm. With the adding of TC, the blue ligand emission decreased rapidly and the  $\text{Eu}^{3+}$  emission enhanced greatly. So a ratiometric method for TC detection was obtained. Both BRH and TC can cause obvious fluorescence color change. Therefore, the as-synthesized Eu-MOF 1 can be used as visual luminescent sensors for BRH and TC.

## Experimental section

### Reagents and chemicals

All materials and solvents were commercially available and were used without further purification. Europium (III) nitrate hexahydrate, berberine hydrochloride (BRH), tetracycline (TC), penicillin G (PEN G), and kanamycin (KANA) were obtained from Aladdin Reagent Co., Ltd. (Shanghai, China). Terephthalic acid was purchased from Shanghai Macklin Biochemical Co., Ltd. Azithromycin (AZM), glutathione (GSH), erythromycin (ERY), 1H-1,2,4-triazole-3,5-diamine (Hdatrz), and streptomycin (STR) were supplied by Adamas Reagent, Ltd. (Shanghai, China). Ultrapure water was prepared with a Millipore system (18.2 M $\Omega$  cm).

### Instrumentation and characterization

Fluorescence experiments were performed by a Hitachi F-7000 fluorescence spectrophotometer (Tokyo, Japan). UV-vis absorption spectra were obtained with a Shimadzu UV-2600 spectrophotometer (Tokyo, Japan). Fourier transform infrared (FTIR) spectra were measured (400–4000  $\text{cm}^{-1}$ ) by a NEXUS-670 FTIR spectrometer (NICOLET, USA). The morphologies of the products were characterized by S-4800 scanning electron microscopy (Hitachi, Japan). The lifetime and fluorescence quantum yield (QY) were achieved from a JY HRIBA FluoroLog-3 (HORIBA, Japan). PXRD patterns were performed using Cu  $\text{K}\alpha_1$  radiation on a Bruker D8 X-ray diffractometer. The EDX mapping images were measured by a talos F200x High Resolution Transmission Electron Microscope. TGA were measured on a Netzsch STA 449C system (Netzsch, Germany) at a heating rate of 10  $^\circ\text{C}/\text{min}$  from 40  $^\circ\text{C}$  temperature to 800  $^\circ\text{C}$  under nitrogen atmosphere.

### Synthesis of Eu-MOF 1 and Eu-MOF 2

Eu-MOF 1 is synthesized by a simple one-pot solvothermal process. Briefly,  $\text{Eu}(\text{NO}_3)_3 \cdot 6\text{H}_2\text{O}$  (0.1 mmol, 44.6 mg), terephthalic acid (0.5 mmol, 83 mg), and Hdatrz (0.3 mmol, 30 mg) were ultrasonically mixed for 30 min containing DMF/ $\text{H}_2\text{O}$  (6:3, 9 mL) solution, then transferred into a 25-mL Teflon-lined autoclave and kept it at 150  $^\circ\text{C}$  for 27 h. After cooling to room temperature, the white solid product was collected by centrifugation and washed with DMF and ethanol for three times, respectively. Finally, the product was dried at 80  $^\circ\text{C}$  for 8 h under vacuum. The synthesis of Eu-MOF 2 is similar to that of Eu-MOF 1, but no 1H-1,2,4-triazole-3,5-diamine is added.

### Luminescent sensing experiments

The Eu-MOF 1 was dissolved in water forming 1 mg/mL suspension by ultrasonication treatment for 30 min. Then the

suspension was applied for fluorescence sensing BRH and TC, respectively. BRH solution was incrementally added to make the final concentration range from 0 to 320  $\mu\text{M}$ ; their fluorescence spectra were recorded at 280-nm excitation after 15-min incubation. The final concentrations of TC were 0, 0.05, 0.5, 1, 5, 10, 20, 40, 60, 80, 120, and 160  $\mu\text{M}$ . After 30-min incubation, the fluorescence spectra were measured at 365-nm excitation. The selectivity of Eu-MOF 1 toward analytes was measured with the concentration of 1.0 mM other substances.

## Results and discussion

### Characterization of Eu-MOF

To demonstrate our strategy, the prepared Eu-MOFs were fully characterized. The SEM image shows that Eu-MOF 1 is lobate and the size is about 6  $\mu\text{m}$  (Fig. 1a). The material morphology is dependent on temperature (see Electronic Supplementary Material (ESM) Fig. S1). However, the reaction time hardly affects its size and morphology (ESM Fig. S2). Therefore, 150  $^{\circ}\text{C}$  and 27 h were selected to prepare Eu-MOF 1 considering the appropriate size and high efficiency. To explore the effect of Hdatrz, Eu-MOF 2 was prepared as a comparison. The PXRD of both Eu-MOF 1 and 2 are in good agreement with the reported MOF [37], which indicates the prepared microparticles are isostructural with the reported MOF and the introduction of Hdatrz did not interfere with the crystal structure of the Eu-MOF 1 (ESM Fig. S3).

FTIR spectra of terephthalic acid, Hdatrz, and Eu-MOF 1 and 2 were investigated. As shown in Fig. 1b, terephthalic acid shows a peak at 1685  $\text{cm}^{-1}$ , which originated from the stretching vibration of C=O in carboxyl groups. However, no peak at 1685  $\text{cm}^{-1}$  is observed in Eu-MOF 1 and 2, indicating carboxylate groups coordinated to  $\text{Eu}^{3+}$ . Compared with Eu-MOF 2, the peaks at 679  $\text{cm}^{-1}$  and 1647  $\text{cm}^{-1}$  in Eu-MOF 1 are

the N-H out-of-plane bending vibration and N-H in-plane bending vibration, respectively [38], clearly indicating the successful modification of Eu-MOF 1 with Hdatrz. The uniform distribution of N in EDX mapping images also proves this statement (ESM Fig. S4). The thermogravimetric analyses (TGA) of Eu-MOF 1 and 2 were measured (ESM Fig. S5), and there are two major weight loss regions. The first weight loss in the range of 160–190  $^{\circ}\text{C}$  is assigned as the loss of solvent molecule. The weight loss in the range of 580–640  $^{\circ}\text{C}$  is attributed to the destruction of the framework. The results indicate that the synthesized Eu-MOFs have a favorable thermal stability. The difference of remaining weight between Eu-MOF 1 and 2 is 4.9%, which is owing to the addition of Hdatrz in Eu-MOF 1 [39].

### Fluorescence properties of Eu-MOFs

To understand the effect of Hdatrz on the emission behavior of Eu-MOF 1, the luminescent spectra of Eu-MOF 1 and 2 were tested (ESM Fig. S6). They have similar fluorescence spectra when excited at 280 nm or 365 nm. However, the QY of Eu-MOF 1 is much higher than that of Eu-MOF 2. Their QYs are 30.99% and 11.91%, respectively (ESM Fig. S7). The experimental results of QYs suggest that Hdatrz works as a highly efficient fluorescence sensitizer [40]. Unfortunately, the single-crystal Eu-MOF 1 is hard to obtain. Thus, it is difficult to explore the detailed mechanisms of how Hdatrz enhanced the QY of Eu-MOF 1 from crystal structure. It is surmised that Hdatrz ligand coordinated to the  $\text{Eu}^{3+}$  center and replaced the coordinated water molecules. Because the vibrational coupling of water molecules will shorten the decay time of  $\text{Eu}^{3+}$  [41], the shorter lifetime of Eu-MOF 2 also confirmed this statement (ESM Fig. S8).

To further study the luminescent properties, Eu-MOF 1 was chosen (Fig. 2a). Under the excitation at 280 nm, the typical transitions  $^5\text{D}_0 \rightarrow ^7\text{F}_1$  (598 nm),  $^5\text{D}_0 \rightarrow ^7\text{F}_2$  (622 nm), and  $^5\text{D}_0 \rightarrow ^7\text{F}_4$  (704 nm) of the  $\text{Eu}^{3+}$  occurred and the CIE (Commission

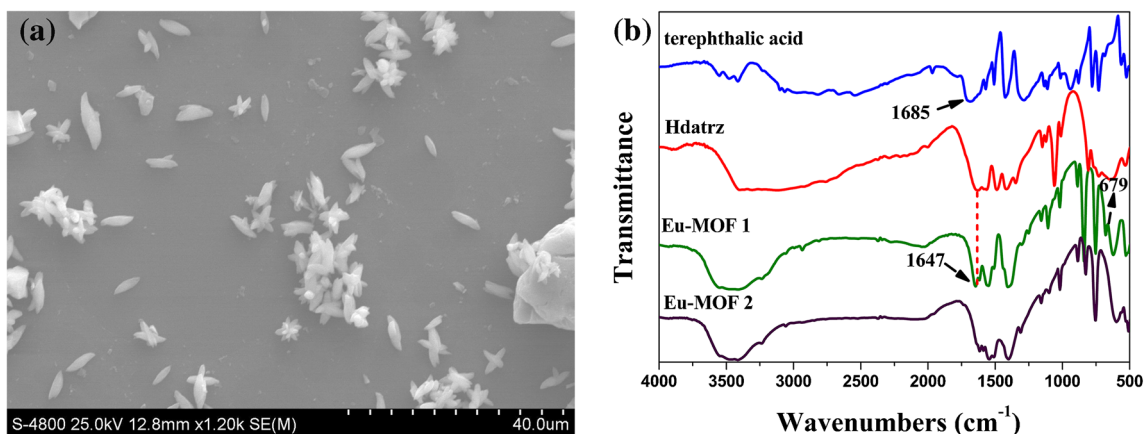


Fig. 1 a SEM image of Eu-MOF 1. b FTIR spectra of Eu-MOF 1, 2 and ligands

Internationale de l'éclairage) coordinate is (0.626, 0.323) (Fig. 2b), which indicates that there is effective energy transfer from ligands to  $\text{Eu}^{3+}$ . In addition, the weak band at 540 nm is attributed to  ${}^5\text{D}_1 \rightarrow {}^7\text{F}_0$  transition of  $\text{Eu}^{3+}$  [42]. The much stronger transition  ${}^5\text{D}_0 \rightarrow {}^7\text{F}_2$  (622 nm) results in strong red emission light of Eu-MOF 1 powder (down) under 254 nm UV lamp and white powder (up) under daylight (Fig. 2a, inset).

It is found that Eu-MOF 1 displays two blue emission peaks at 420 and 480 nm with CIE coordinates of (0.184, 0.168) when excitation wavelength is 365 nm (Fig. 2a, b). One of the blue emissions centered at 480 nm may be ascribe to the ligand-to-metal charge transfer (LMCT) and/or metal-to-ligand charge transfer (MLCT) [43]. Another blue emission of Eu-MOF 1 at 420 nm is consistent with free ligands (ESM Fig. S9). It suggests that the blue emission at 420 nm derives from  $\pi-\pi^*$  transition of ligands. Meanwhile, the characteristic emission bands of  $\text{Eu}^{3+}$  are very weak with an excitation of 365 nm (Fig. 2a), which is attributed to poor efficient energy transfer between ligands and metal ions. A process of tunable emission spectra from single-emission to dual-emission could be observed when varying excitation wavelength from 280 to 365 nm. To study the stability, the fluorescence intensity of Eu-MOF 1 after a month of storage in water was measured (ESM Fig. S10). The results show a good water-dispersibility and fluorescence stability in water.

Based on the above, Eu-MOF 1 is expected to be a multi-functional fluorescent visual sensor.

## Sensing of BRH

Considering the excellent fluorescence properties, the prepared Eu-MOF 1 was used for sensing BRH (ESM Fig. S11). The fluorescence signal is quenched remarkably by BRH under the

excitation at 280 nm. The experimental conditions were optimized (ESM Fig. S12). To evaluate the sensitivity of Eu-MOF 1 toward BRH, BRH with different concentrations were added. As shown in Fig. 3a, the fluorescence intensity has a remarkable response to BRH with a maximum quench percentage of 96.7%. The corresponding CIE coordinates are shown in Fig. 3b. The working curve was obtained by plotting  $(F_0-F)/F_0$  against the BRH concentration, and it satisfies the exponential regression curve with a broad linear range from 0.5–320  $\mu\text{M}$  ( $R^2 = 0.9988$ , LOD = 78 nM) (Fig. 3c).  $F_0$  and  $F$  are fluorescent intensities without and with BRH. An obvious change of fluorescence color from red to orange and then green is observed with the increase of BRH concentration under UV lamp of 254 nm excitation (Fig. 3a, inset), which attribute to the reference fluorescence signal at 545 nm of BRH. Thus, a visual determination of BRH can be achieved with low-cost UV lamp.

The selectivity of this method was investigated by the addition of BRH and common cations ( $\text{Cd}^{2+}$ ,  $\text{Ag}^+$ ,  $\text{Hg}^+$ ,  $\text{Ca}^{2+}$ ,  $\text{Ba}^{2+}$ ,  $\text{K}^+$ ,  $\text{Ni}^{2+}$ ,  $\text{Pb}^{2+}$ ,  $\text{Zn}^{2+}$ ,  $\text{Mn}^{2+}$ ,  $\text{Mg}^{2+}$ ,  $\text{Cr}^{3+}$ ,  $\text{Co}^{2+}$ ,  $\text{Na}^+$ , and  $\text{NH}_4^+$ ), anions ( $\text{SCN}^-$ ,  $\text{SO}_4^{2-}$ ), natural amino acids (glycine, L-cysteine, L-histidine, L-lysine, arginine, and GSH) and saccharides (glucose, sucrose, and starch). As shown in Fig. 3d, Eu-MOF 1 has significant emission intensity change only in the presence of 160  $\mu\text{M}$  BRH. The negligible changes of fluorescence intensity caused by 1 mM substances indicate the outstanding selectivity for BRH detection (Fig. 3e). And no interference is observed in Fig. S13 (see ESM). Therefore, the developed method for sensing BRH has a good selectivity and anti-interference ability.

## Fluorescent ratiometry for TC

To demonstrate the multi-mode analytical application, Eu-MOF 1 was used for TC sensing under excitation at 365 nm.

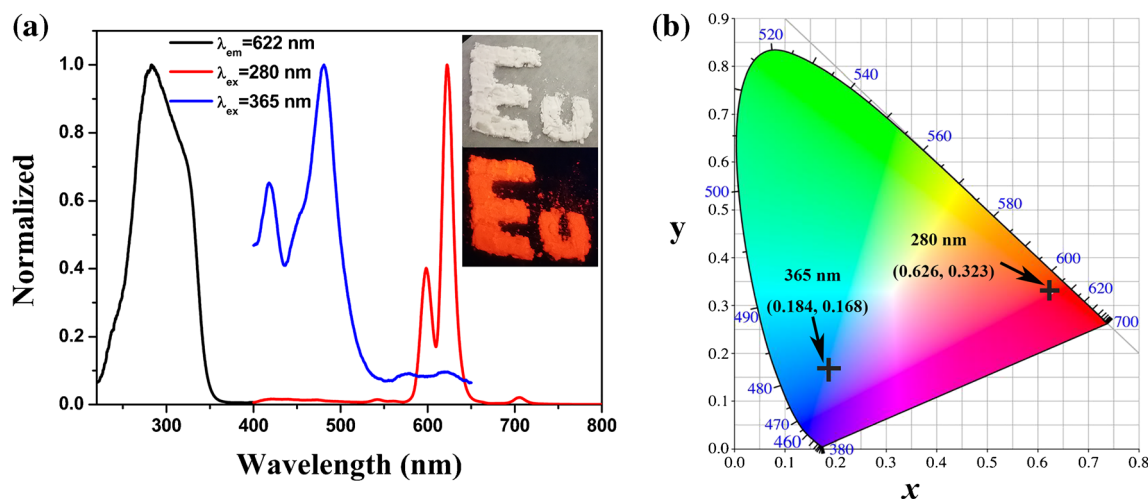


**Fig. 2** **a** Excitation and emission spectra of Eu-MOF 1; inset, photograph of Eu-MOF 1 powder under daylight (up) and 254 nm UV lamp (down). **b** CIE coordinates of Eu-MOF 1 under different excitation

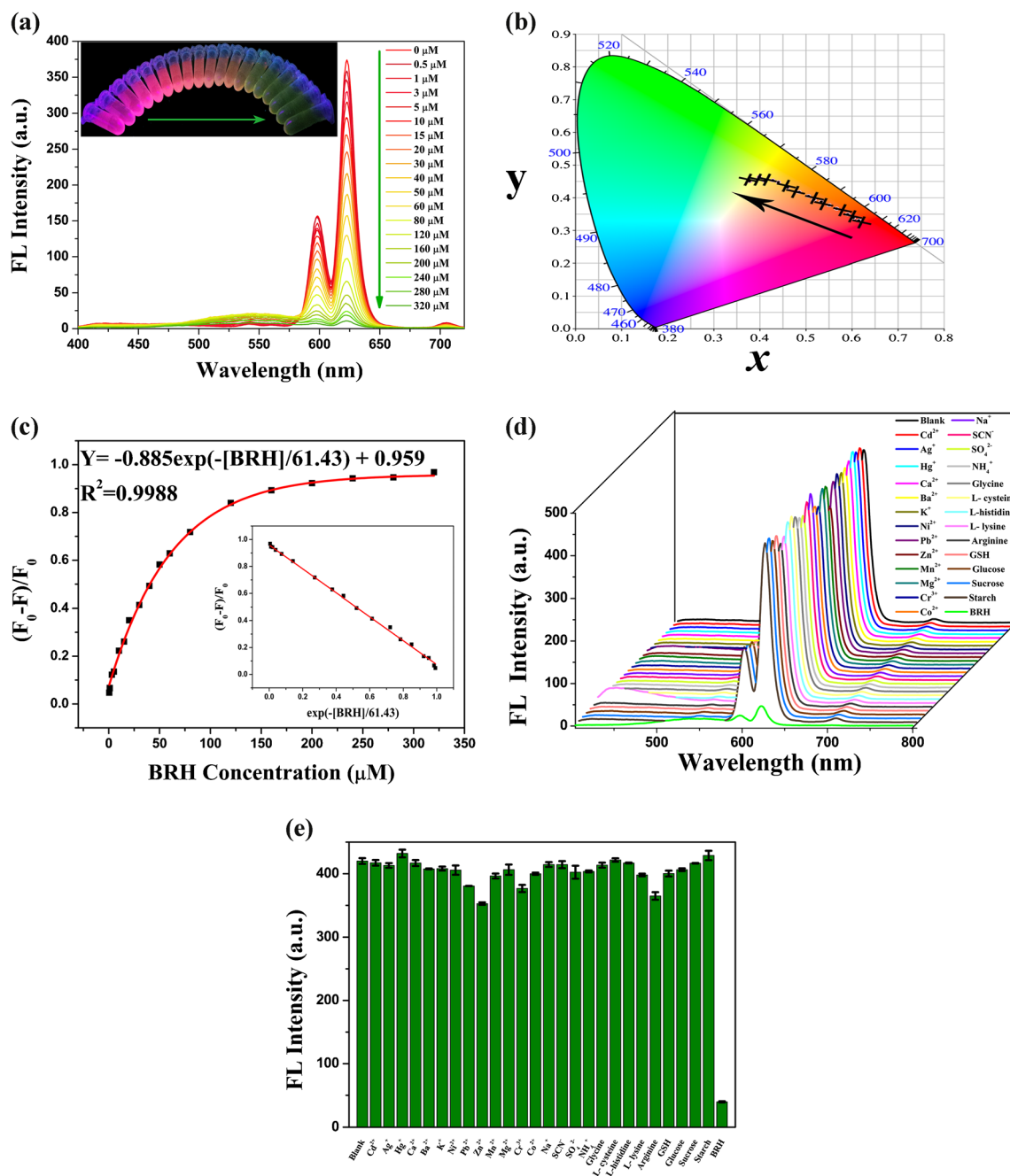


**Fig. 3** **a** Emission spectra ( $\lambda_{\text{ex}} = 280 \text{ nm}$ ) of Eu-MOF 1 - BRH. The inset is the photograph (254 nm UV lamp). **b** CIE coordinates. **c** Plot of  $(F_0 - F)/F_0$  versus BRH concentration. Fluorescence spectra (**d**) and intensity (**e**) of Eu-MOF 1 with BRH (160  $\mu\text{M}$ ) and substances (1 mM)

The experimental conditions were optimized firstly (ESM Fig. S14). Eu-MOF 1 shows the blue emission of ligands at 480 nm and the weak red emission of  $\text{Eu}^{3+}$  at 622 nm in the absence of TC (ESM Fig. S15). After addition of TC, the emission of ligands was reduced while the typical emission of  $\text{Eu}^{3+}$  was enhanced; this can be used for fluorescent ratio analysis of TC (Fig. 4a). And a fluorescence color change from nattier blue to red is observed, which is easily identified by naked eyes (Fig. 4a, inset). The corresponding CIE coordinates are shown in Fig. 4b. The fluorescence intensity ratio

response for TC is better than that of single fluorescence signal (ESM Fig. S16). A decreasing trend of the fluorescence intensity of  $\text{Eu}^{3+}$  ions at 622 nm after 160  $\mu\text{M}$  ascribes to the concentration quenching (ESM Fig. S16b). The fluorescence intensity ratio of  $F_{622}/F_{480}$  was recorded with the TC concentration ranging from 0 to 280  $\mu\text{M}$  (ESM Fig. S17). However, a good linear relationship ( $R^2 = 0.9969$ ) was obtained in the range from 0.05 to 160  $\mu\text{M}$  (Fig. 4c). The limit of detection is 17 nM. In addition, we also compared various methods for the detection of TC (ESM Table S1). Our method shows low

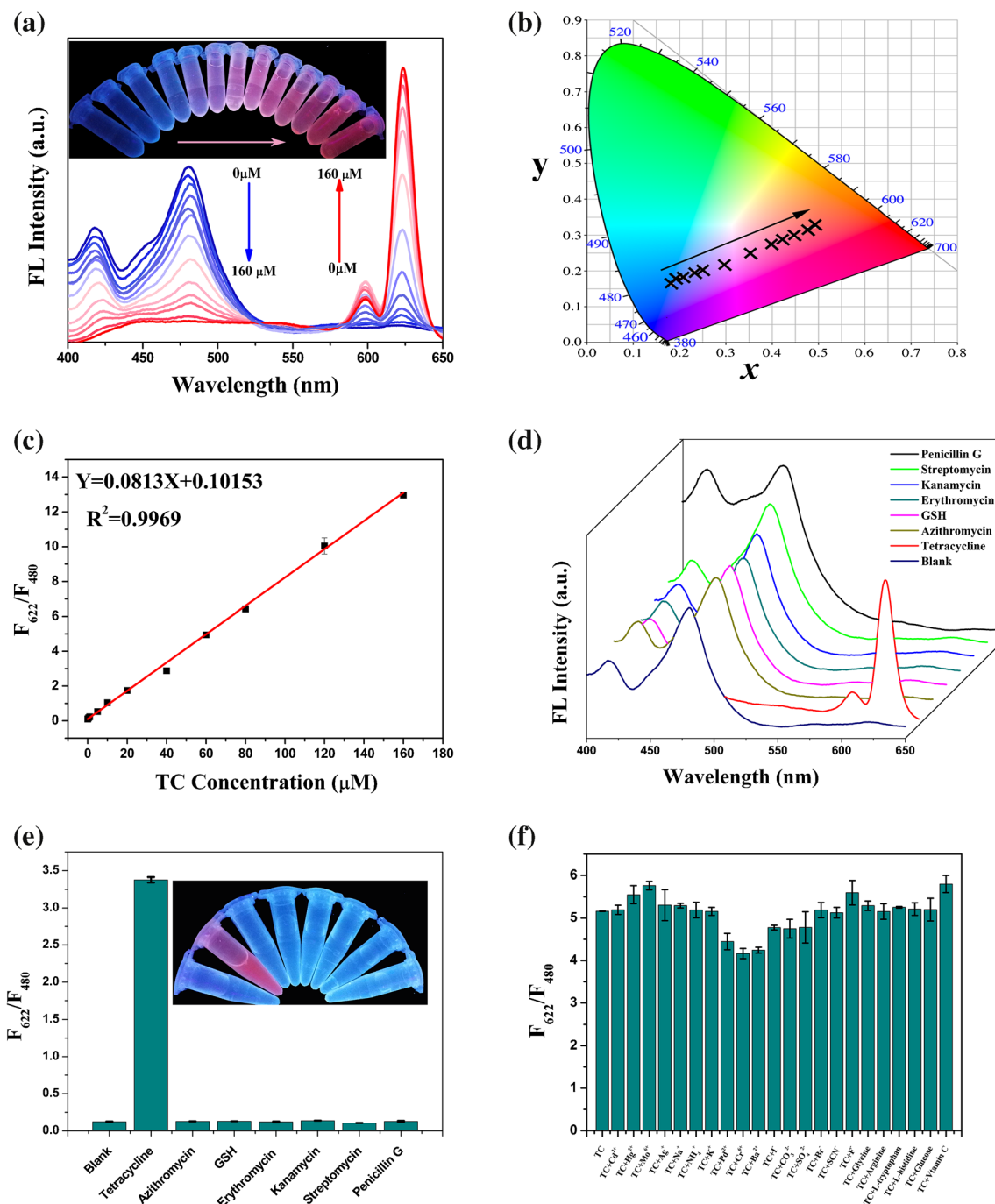


**Fig. 4** **a** Fluorescence spectra ( $\lambda_{\text{ex}} = 365 \text{ nm}$ ) of Eu-MOF 1 - TC. The inset is the photograph. **b** CIE coordinates. **c** Plot of  $F_{622}/F_{480}$  versus TC concentration. The selectivity fluorescence spectra (**d**) and intensity ratio

of  $F_{622}/F_{480}$  (**e**) of Eu-MOF 1 with TC (80  $\mu\text{M}$ ) and other antibiotics (1 mM). **f** The interference experiment (80  $\mu\text{M}$  TC and 1 mM other antibiotics)

detection limit, ratiometric signal, visual sensing, and easy operation.

To validate the selectivity of TC sensing, the fluorescence intensities of Eu-MOF 1 in the presence of other antibiotics (azithromycin, GSH, erythromycin, kanamycin, streptomycin, and penicillin G) were recorded (Fig. 4d, e). Only TC shows the significant fluorescence

intensity change. And it is easy to recognize with the naked eye (Fig. 4e, inset). A notable fluorescence ratio intensity change occurred from other antibiotics after the addition of TC (ESM Fig. S18). Furthermore, no interference is observed in the presence of interfering substrates (glycine, arginine, L-tryptophan, L-histidine, glucose, and vitamin C) and foreign ions ( $\text{Cd}^{2+}$ ,  $\text{Hg}^{2+}$ ,  $\text{K}^+$ ,

**Table 1** Results of determination of BRH in real samples

Sample	Added ( $\mu\text{M}$ )	Found ( $\mu\text{M}$ )	RSD (%)	Recovery (%)	
Urine	5	5.56, 5.47, 5.39, 5.36, 5.45	1.36	107.1–110.9	
	20	20.27, 20.08, 20.56, 20.76, 19.98	1.61	99.9–103.8	
	80	79.26, 81.57, 77.08, 77.69, 76.00, 78.32	2.78	95.0–102.0	
	Label claim (mg tablet <sup>-1</sup> )	The proposed method		HPLC method	
Tablets*		Found (mg tablet <sup>-1</sup> )	RSD (%)	Found (mg tablet <sup>-1</sup> )	RSD (%)
	40	39.73, 42.07, 40.66, 40.29, 39.82	2.34	39.84, 40.05, 40.12, 39.09, 39.64	1.04

\*Fufang Huangliansu Pian is made in Taiji Pharmaceutical Ltd., Chongqing, China

$\text{Na}^+$ ,  $\text{NH}_4^+$ ,  $\text{Ag}^+$ ,  $\text{Mo}^{6+}$ ,  $\text{Pd}^{2+}$ ,  $\text{Ba}^{2+}$ ,  $\text{Cr}^{6+}$ ,  $\text{F}^-$ ,  $\text{Cl}^-$ ,  $\text{SCN}^-$ ,  $\text{I}^-$ ,  $\text{CO}_3^{2-}$ ,  $\text{SO}_4^{2-}$ , and  $\text{NO}_3^-$ ; see Fig. 4f). The results demonstrate that Eu-MOF 1 has a good selectivity for the ratiometric determination of TC.

### Mechanism of sensing

As for the fluorescence quenching of Eu-MOF 1 by BRH, the main reasons are competitive absorption of the light source energy and energy transfer.

The PXRD pattern of Eu-MOF 1 after treatment with BRH is shown in Fig. S3 (see ESM). The result shows that the crystal structure still keeps integrity, which confirms that the fluorescence quenching is not caused by the collapse of framework. The UV-Vis absorption spectrum of BRH was also studied (ESM Fig. S19). The moderate overlap between the absorption spectrum of BRH and the excitation spectrum of Eu-MOF 1 indicates the competitive absorption of the light source energy between them. In addition, recyclability experiment was investigated (Fig. 5a). The fluorescence intensity revert to only 52% of the initial state after the cycle performed five times. This might be caused by the energy transfer and the

remnant of BRH. Besides, BRH has an electron-pulling pyridine ring (ESM Scheme S1), which can induce an electron-transfer process from Eu-MOF 1 to pyridine ring and consequently results in an emission quenching [39]. As shown in Fig. S8 (see ESM), the fluorescence lifetime ( $\tau$ ) of Eu-MOF 1 with BRH has a negligible change as compared with original suspension, which is consistent with the decrease of fluorescence intensity and reveals the existence of static quenching process. Thus, the quenching procedure of this system shall be attributed to competitive absorption of the light source energy and energy transfer.

To discuss the mechanism of Eu-MOF 1 towards TC, the UV-Vis absorption spectra of Eu-MOF 1, TC, and Eu-MOF 1-TC were studied (Fig. 5b). TC has a strong absorption peak at 365 nm. Compared with the absorption spectrum of Eu-MOF 1, the absorption peak of Eu-MOF 1-TC has a new peak at 390 nm. The red shift of the absorption peak reveals that a new complex of Eu-MOF 1-TC is formed. The longer fluorescence lifetime ( $\tau$ ) of Eu-MOF 1-TC also confirms this statement (ESM Fig. S8). According to the reported research, TC can coordinate with  $\text{Eu}^{3+}$  and has an excellent “antenna effect” [44]. Thus, the emission enhancement of  $\text{Eu}^{3+}$  can be ascribed to the absorbed

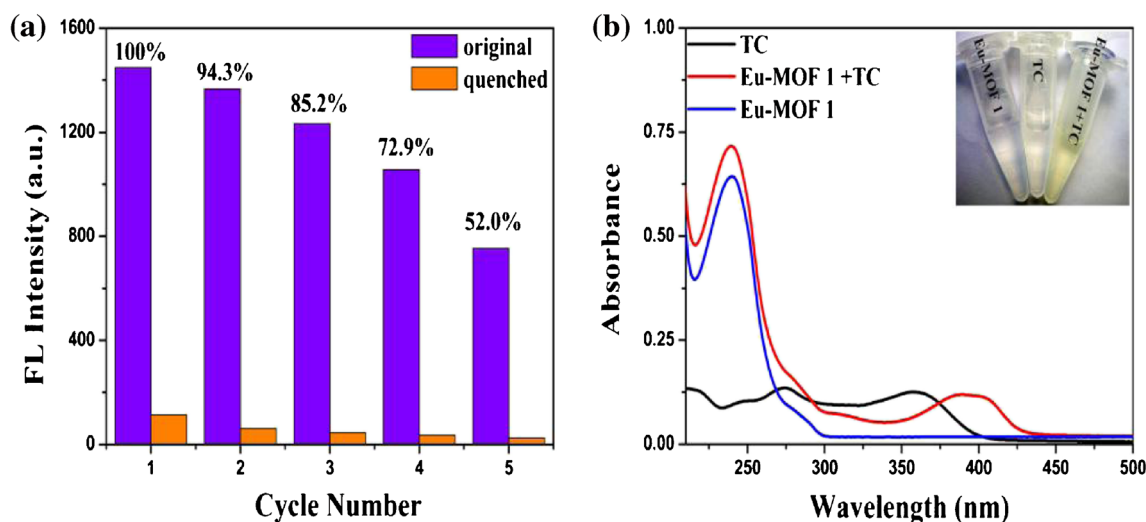


**Fig. 5** a Reproducibility application. b The absorption spectra of TC, Eu-MOF 1, and Eu-MOF 1 - TC

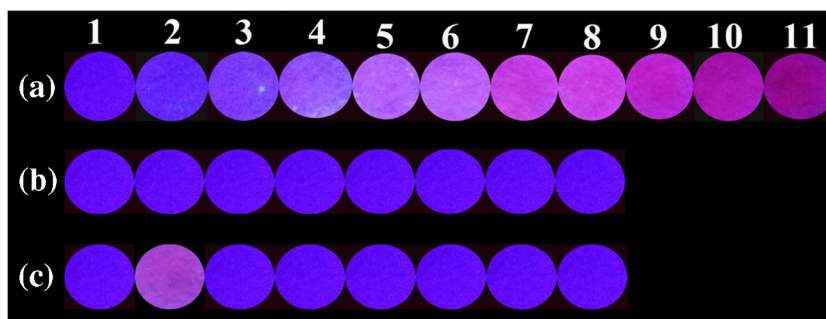


**Fig. 6** Eu-MOF 1-based paper sensor for visual detection TC (365 nm UV lamp). Photographs (a) of Eu-MOF 1 with TC (from 1 to 11: 0, 1, 3, 5, 10, 20, 40, 60, 80, 120, and 160  $\mu\text{M}$ ); photographs (b) of Eu-MOF 1;

photographs (c) of Eu-MOF 1 contains 80  $\mu\text{M}$  TC and 1 mM other antibiotics (from 1 to 8: blank, TC, azithromycin, GSH, erythromycin, kanamycin, streptomycin, and penicillin G)

energy transfer from TC to Eu-MOF 1. In addition, we investigated the effects of TC on the fluorescence of the ligand-center emission. Upon the addition of TC, the red shift of the ligand-center emission implies an increase in the  $\pi^*$  orbits of the ligand. Then the more efficiency energy transfer from the ligands to  $\text{Eu}^{3+}$  occurred owing to a better match between the  $\pi^*$  orbits of the ligands and the resonance energy level of  $\text{Eu}^{3+}$  [45]. Therefore, the fluorescence intensity of ligand decreased significantly with a simultaneous fluorescence enhancement of  $\text{Eu}^{3+}$  in the presence of TC.

### Analytical application in real samples

To evaluate its applicability, the proposed method was used to detect BRH in real samples (Table 1). For the human urine, the recoveries are between 99.41 and 109.20%. The founded content in tablet by the method is consistent with the results from the HPLC method [46] and the reference value of 40.00  $\text{mg tablet}^{-1}$ . The Eu-MOF 1 probe was applied to detect TC in river water samples and human serum samples. As listed in Table 2, the added standard TC solution could be measured with good recoveries. Therefore, the results indicate that the proposed method is reliable and practical.

### Visual sensing of TC

We designed a filter paper sensor for the simple and visual detection of TC (ESM Fig. S20). With the increase of TC

concentration, the visual paper probe shows an obvious color gradient from blue to red under the UV lamp irradiation (365 nm) (Fig. 6a). An obvious fluorescent color change is observed by naked eyes even with 3  $\mu\text{M}$  TC. The phenomenon is similar to the fluorescent color change in aqueous solution, which reveals that the test strip also has a good sensitivity. Furthermore, the selectivity of the filter paper sensor was also studied. It can be seen that only TC can change the fluorescent color (Fig. 6b, c). These results indicate that the prepared paper sensor can be used for the facile and rapid visual detection of TC.

### Conclusion

In summary, we successfully synthesized Eu-MOF with high quantum yield, excellent fluorescence stability, and favorable thermal stability. The prepared Eu-MOF was used as a dual-mode probe for the rapid, sensitive, selective, and visual sensing of BRH and TC. The assay of BRH is based on the fluorescence quenching when excited at 280 nm. And the TC sensing is achieved by fluorescence ratio method at 365 nm excitation. Both of the two methods can realize visual detection. A filter paper sensor for visual sensing TC based on Eu-MOF was successfully designed, which can be used conveniently to monitor TC in environment water and biological system. This work provides a new strategy for the design of multi-mode fluorescent sensors.

**Table 2** Results of determination of TC in real samples

Sample	Added ( $\mu\text{M}$ )	Found ( $\mu\text{M}$ )	RSD (% , $n=5$ )	Recovery (% , $n=5$ )
River water	5	5.31, 5.61, 5.63, 5.61, 5.28	3.20	105.7–112.6
	20	18.55, 18.65, 19.84, 19.52, 19.79	3.24	92.8–99.2
	80	77.02, 75.14, 78.53, 74.56, 75.03	2.19	93.2–98.2
Human serum	1	1.01, 1.00, 1.02, 1.00, 1.03	1.22	100.0–103.0
	5	5.35, 5.48, 5.32, 5.44, 5.49	1.45	106.3–109.8
	20	21.54, 20.81, 21.78, 21.27, 21.24	1.70	104.1–108.9



**Funding information** This study received financial support from the National Natural Science Foundation of China (NSFC, No. 21377103).

## Compliance with ethical standards

**Ethical standards and informed consent** This work was approved by The Laboratory Animal Ethics Review Committee for Southwest University and was performed in accordance with ethical standards. Informed consent was obtained from all individual participants included in the study.

**Conflict of interest** The authors declare that they have no conflict of interest.

## References

- Kuo CL, Chi CW, Liu TY. The anti-inflammatory potential of berberine in vitro and in vivo. *Cancer Lett.* 2004;203:127–37.
- Zhou JY, Zhou SW, Tang JL, Zhang KB, Guang LX, Huang YP, et al. Protective effect of berberine on beta cells in streptozotocin- and high-carbohydrate/high-fat diet-induced diabetic rats. *Eur J Pharmacol.* 2009;606:262–8.
- Zhang XB, Li ZZ, Guo CC, Chen SH, Shen GL, Yu RQ. Porphyrin-metalloporphyrin composite based optical fiber sensor for the determination of berberine. *Anal Chim Acta.* 2001;439:65–71.
- Shrinivas SK, Ashish D. On the mechanism of antidepressant-like action of berberine chloride. *Eur J Pharmacol.* 2008;589:163–72.
- Domadia PN, Bhunia A, Sivaraman J, Swarup S, Dasgupta D. Berberine targets assembly of escherichia coli cell division protein FtsZ. *Biochemistry.* 2008;47:3225–34.
- Wang JC, Zhang Q, Cai DF. Stability-indicating validated HPLC method for analysis of berberine hydrochloride and trimethoprim in pharmaceutical dosage form. *J Chem.* 2013;9:360812.
- Biparva P, Abedirad SM, Kazemi SY, Shanehsaz M. Chemiluminescence recognition of berberine triggered by biomimetically synthesized silver nanoparticles. *Sensors Actuators B Chem.* 2016;234:278–85.
- Ling J, Sang Y, Huang CZ. Visual colorimetric detection of berberine hydrochloride with silver nanoparticles. *J Pharm Biomed Anal.* 2008;47:860–4.
- Uzasci S, Erim FB. Enhancement of native fluorescence intensity of berberine by (2-hydroxypropyl)-cyclodextrin in capillary electrophoresis coupled by laser-induced fluorescence detection: application to quality control of medicinal plants. *J Chromatogr A.* 2014;1338:184–7.
- Pang XB, Huang CZ. A selective and sensitive assay of berberine using total internal reflected resonance light scattering technique with fluorescein at the water/1,2-dichloroethane interface. *J Pharm Biomed Anal.* 2004;35:185–91.
- Schnappinger D, Hillen W. Tetracyclines: antibiotic action, uptake, and resistance mechanisms. *Arch Microbiol.* 1996;165:359–69.
- Ferri M, Ranucci E, Romagnoli P, Giaccone V. Antimicrobial resistance: a global emerging threat to public health systems. *Crit Rev Food Sci Nutr.* 2017;57:2857–76.
- Liu Y, Yang HL, Yang S, Hu QW, Cheng HB, Liu HY, et al. High-performance liquid chromatography using pressurized liquid extraction for the determination of seven tetracyclines in egg, fish and shrimp. *J Chromatogr B.* 2013;917:11–7.
- Ibarra IS, Rodriguez JA, Miranda JM, Vega M, Barrado E. Magnetic solid phase extraction based on phenyl silica adsorbent for the determination of tetracyclines in milk samples by capillary electrophoresis. *J Chromatogr A.* 2011;1218:2196–202.
- Nebot C, Guarddon M, Seco F, Iglesias A, Miranda JM, Franco CM, et al. Monitoring the presence of residues of tetracyclines in baby food samples by HPLC-MS/MS. *Food Control.* 2014;46:495–501.
- Taghdisi SM, Danesh NM, Ramezani M, Abnous K. A novel M-shape electrochemical aptasensor for ultrasensitive detection of tetracyclines. *Biosens Bioelectron.* 2016;85:509–14.
- Le T, Yu H, Zhao ZW, Wei W. Development of a monoclonal antibody-based ELISA for the detection of oxytetracycline and 4-epi-oxytetracycline residues in chicken tissues. *Anal Lett.* 2012;45:386–94.
- Wang YL, Sun YJ, Dai HC, Ni PJ, Jiang S, Lu WD, et al. A colorimetric biosensor using Fe<sub>3</sub>O<sub>4</sub> nanoparticles for highly sensitive and selective detection of tetracyclines. *Sensors Actuators B Chem.* 2016;236:621–6.
- Miao H, Wang YY, Yang XM. Carbon dots derived from tobacco for visually distinguishing and detecting three kinds of tetracyclines. *Nanoscale.* 2018;10:8139–45.
- Zhu XD, Zhang K, Wang Y, Long WW, Sa RJ, Liu TF, et al. Fluorescent metal-organic framework (MOF) as a highly sensitive and quickly responsive chemical sensor for the detection of antibiotics in simulated wastewater. *Inorg Chem.* 2018;57:1060–5.
- Yang QY, Liu DH, Zhong CL, Li JR. Development of computational methodologies for metal-organic frameworks and their application in gas separations. *Chem Rev.* 2013;113:8261–323.
- Li GQ, Kobayashi H, Taylor JM, Ikeda R, Kubota Y, Kato K, et al. Hydrogen storage in Pd nanocrystals covered with a metal-organic framework. *Nat Mater.* 2014;13:802–6.
- Xiong YH, Chen SH, Ye FG, Su LJ, Zhang C, Shen SF, et al. Synthesis of a mixed valence state Ce-MOF as an oxidase mimetic for the colorimetric detection of biothiols. *Chem Commun.* 2015;51:4635–8.
- Jiang XJ, Liu XH, Wu TD, Li L, Zhang RJ, Lu XQ. Metal-organic framework derived carbon-based sensor for monitoring of the oxidative stress of living cell and assessment of antioxidant activity of food extracts. *Talanta.* 2019;194:591–7.
- Hu GB, Xiong CY, Liang WB, Zeng XS, Xu HL, Yang Y, et al. Highly stable mesoporous luminescence-functionalized MOF with excellent electrochemiluminescence property for ultrasensitive immunosensor construction. *ACS Appl Mater Interfaces.* 2018;10:15913–9.
- Cui YJ, Chen BG, Qian GD. Lanthanide metal-organic frameworks for luminescent sensing and light-emitting applications. *Coord Chem Rev.* 2014;173:76–86.
- Cui YJ, Yue YF, Qian GD, Chen BG. Luminescent functional metal organic frameworks. *Chem Rev.* 2012;112:1126–62.
- Wang XN, Li JL, Jiang CJ, Hu P, Li B, Zhang TL, et al. An efficient strategy for improving the luminescent sensing performance of a terbium(III) metal-organic framework towards multiple substances. *Chem Commun.* 2018;54:13271–4.
- Li HH, Han YB, Shao ZC, Li N, Huang C, Hou HW. Water-stable Eu-MOF fluorescent sensors for trivalent metal ions and nitrobenzene. *Dalton Trans.* 2017;46:12201–8.
- Niu WF, Guo L, Li YH, Shuang SM, Dong C, Wong MS. Highly selective two-photon fluorescent probe for ratiometric sensing and imaging cysteine in mitochondria. *Anal Chem.* 2016;88:1908–14.
- Wu JK, Ma JW, Wang H, Qin DM, An L, Ma Y, et al. Rapid and visual detection of benzothiostrubin residue in strawberry using quantum dot-based lateral flow test strip. *Sensors Actuators B Chem.* 2019;283:222–9.
- Kang Y, Zheng XJ, Jin LP. A microscale multi-functional metal-organic framework as a fluorescence chemosensor for Fe(III), Al(III) and 2-hydroxy-1-Naphthaldehyde. *J Colloid Interface Sci.* 2016;471:1–6.
- Zhang SY, Shi W, Cheng P, Zaworotko MJ. A mixed-crystal lanthanide zeolite-like metal-organic framework as a fluorescent

- indicator for lysophosphatidic acid, a cancer biomarker. *J Am Chem Soc.* 2015;137:12203–6.
34. Wang L, Fan GL, Xu XF, Chen DM, Wang L, Shi W, et al. Detection of polychlorinated benzenes (persistent organic pollutants) by a luminescent sensor based on a lanthanide metal-organic framework. *J Mater Chem A.* 2017;5:5541–9.
  35. Wu LL, Zhao JF, Wang H, Wang JY. A lanthanide(III) metal-organic framework exhibiting ratiometric luminescent temperature sensing and tunable white light emission. *CrystEngComm.* 2016;18:4268–71.
  36. Xia TF, Cui YJ, Yang Y, Qian GD. Highly stable mixed-lanthanide metal-organic frameworks for self-referencing and colorimetric luminescent pH sensing. *ChemNanoMat.* 2017;3:51–7.
  37. Reineke TM, Eddaoudi M, Fehr M, Kelley D, Yaghi OM. From condensed lanthanide coordination solids to microporous frameworks having accessible metal sites. *J Am Chem Soc.* 1999;121:1651–7.
  38. Cai LL, Wang BZ, Jiao L, Ge ZX, Qin GM, Li H. Study on synthetic reaction mechanism of 3,5-diamino-1,2,4-triazole by chemometrics and infrared spectroscopy. *Chin J Anal Chem.* 2011;39:920–4.
  39. Shi KY, Yang ZC, Dong LH, Yu B. Dual channel detection for anthrax biomarker dipicolinic acid: the combination of an emission turn on probe and luminescent metal-organic frameworks. *Sensors Actuators B Chem.* 2018;266:263–9.
  40. Kang J, Chen YN, Wang AL, Li HY, Qu YR, Zhang HX, et al. Synthesis, characterization and luminescent properties of europium complexes with 2,4,6-tris-(2-pyridyl)-s-triazine as highly efficient sensitizers. *Luminescence.* 2015;30:1360–6.
  41. You LX, Zhao BB, Liu HJ, Wang SJ, Xiong G, He YK, et al. 2D and 3D lanthanide metal-organic frameworks constructed from three benzenedicarboxylate ligands: synthesis, structure and luminescent properties. *CrystEngComm.* 2018;20:615–23.
  42. Wu SY, Lin YN, Liu JW, Shi W, Yang GM, Cheng P. Rapid detection of the biomarkers for carcinoid tumors by a water stable luminescent lanthanide metal-organic framework sensor. *Adv Funct Mater.* 2018;28:1707169.
  43. Wang XW, Chen JZ, Liu JH. Photoluminescent Zn(II) metal-organic frameworks built from tetrazole ligand: 2D four-connected regular honeycomb (4363)-net. *Cryst Growth Des.* 2017;7:1227–9.
  44. Ghorai SK, Samanta SK, Mukherjee M, Sardar PS, Ghosh S. Tuning of “antenna effect” of Eu(III) in ternary systems in aqueous medium through binding with protein. *Inorg Chem.* 2013;52:1476–87.
  45. Wang XY, Yao X, Huang Q, Li YX, An GH, Li GM. Triple-wavelength-region luminescence sensing based on a color-tunable emitting lanthanide metal organic framework. *Anal Chem.* 2018;90:6675–82.
  46. The Pharmacopeia Committee of Ministry of Health PR China. The pharmacopeia of PR China, vol. 2. Beijing: China medical science Press; 2015. p. 1243.

**Publisher's note** Springer Nature remains neutral with regard to jurisdictional claims in published maps and institutional affiliations.



**Jie Xiong** received her Bachelor's degree in 2017 from Southwest University. Now she is a post-graduate at Southwest University and her current research interest mainly focuses on sensing application of lanthanide metal-organic framework.



**Lu Yang** is an undergraduate at Southwest University. Her research interest is to synthesize lanthanide metal-organic framework.



**Li Xia Gao** is a master student at Southwest University. Her current research interest focuses on preparation and sensing application of carbon dots.



**Pan Pan Zhu** received her Bachelor's degree in 2016 from Shanxi Normal University. Now she is a master student at Southwest University and her current research interest is preparation and sensing application of carbon dots.



**Ke Jun Tan** is a Professor of Analytical Chemistry at Southwest University. He graduated from the Department of Chemistry, Southwest Normal University in 1991. His research interests include mainly separation and analysis of environmental pollutants, synthesis and application of nanomaterials, and analysis of biochemical drug.



**Qian Chen** is a master student at Southwest University. Her current research field deals with development of fluorescent material for sensing perfluorochemicals.